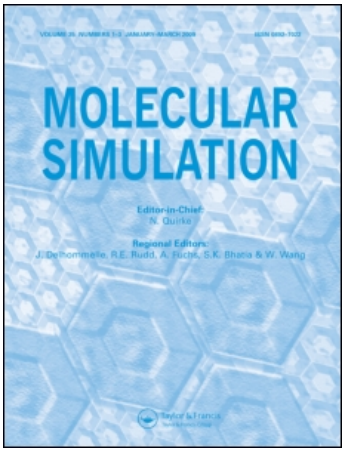

Molecular Simulation
Publication details, including instructions for authors and subscription information:
http://www.informaworld.com/smpp/title~content=t713644482

2D quantum mechanical device modeling and simulation: Centre-channel (CC) and double-gate (DG) MOSFET

K. -D. Kim[a]; T. -Y. Won[a]
[a] Department of Electrical Engineering, School of Engineering, Inha University, Nam-gu, Incheon, Korea

To cite this Article Kim, K. -D. and Won, T. -Y.(2005) '2D quantum mechanical device modeling and simulation: Centre-channel (CC) and double-gate (DG) MOSFET', Molecular Simulation, 31: 12, 825 — 830
To link to this Article: DOI: 10.1080/08927020500314076
URL: http://dx.doi.org/10.1080/08927020500314076

Molecular Simulation, Vol. 31, No. 12, 15 October 2005, 825–830

Taylor & Francis
Taylor & Francis Group

2D quantum mechanical device modeling and simulation: Centre-channel (CC) and double-gate (DG) MOSFET

K.-D. KIM and T.-Y. WON*

Department of Electrical Engineering, School of Engineering, Inha University, 253 Yonghyun-dong, Nam-gu, Incheon 402-751, Korea

(Received May 2005; in final form August 2005)

In this paper, a novel device structure ($Si_{1-x}Ge_x$/Si/$Si_{1-x}Ge_x$ hetero-structure), which is named as "center-channel (CC) double-gate (DG) MOSFET," is proposed. Device performance of the proposed FET structure was investigated with our two-dimensional quantum-mechanical simulator which produces a self-consistent solution of Poisson–Schrödinger equations and the current continuity equation. The CC operation of CC-NMOS is confirmed from the electron density distribution and the band lineups as well as the lowest energy wave function. Current–voltage characteristics including the trans-conductance (G_m) of CC-MOSFET are carefully compared with those of the conventional DG-NMOS to evaluate the distinct feature of the proposed FET structure. Our simulation revealed that the proposed FET demonstrates the enhanced (about ($\sim 1.6\times$) current drive and 60% G_m. Finally, the short-channel effects of CC and DG MOSFET, both of which demonstrate excellent sub-threshold behaviors and open the possibility of device scaling down to sub-20 nm.

Keywords: Quantum-mechanical simulation; Center-Channel operation; double-gate MOSFET; Short-channel effects; Coupled Poisson–Schrödinger equations

1. Introduction

Recent approaches for nano-scale semiconductor devices place a lot of emphasis on materials and structures [1–3]. The enhancement of carrier mobility in the conduction channel needs high-mobility materials such as $Si_{1-x}Ge_x$ and strained-Si. However, conventional MOSFET with strained-Si channel has some disadvantages such as the limit of scaling, high-electric field in the channel, and corresponding degradation of mobility. For the solution of these problems, we propose a high-performance center-channel (CC) double-gate (DG) structure incorporating with the materials of $Si_{1-x}Ge_x$ and strained-Si. To fulfill the numerical simulation of nano-scale structures such as DG MOSFET, we need to obtain a self-consistent solution of the coupled Poisson–Schrödinger equations. The CC-NMOS device exhibits the enhanced current drive and improved switching speed due to the decrease of surface roughness scattering and mobility enhancement of strained-Si channel.

In this paper, we discuss our self-consistent QM investigation for the analysis of CC-NMOSFET. The electrical characteristic of CC-NMOS was carefully investigated in terms of channel length (L_g) (10–80 nm) and gate oxide thickness (T_{ox}) 2 nm. Device optimizations were performed in an effort to suppress the short-channel effects (SCE) through some critical parameters such as subthreshold swing, threshold-voltage (V_t) roll-off and drain-induced barrier lowering (DIBL). At the same time, the differences between the CC-NMOS and DG-NMOS simulation results and especially enhancement of current drive were examined by comparing the band lineups, lowest energy wavefunction, and electron density.

2. Numerical model

Two-dimensional (2D) QM model for describing the effect of strain on the band structure of Si and bound states is based on the self-consistent solution of coupled Poisson–Schrödinger equations [4]:

$$\nabla \cdot [\varepsilon(x,y)\nabla\Phi(x,y)] = -\rho(x,y) \tag{1}$$

$$\rho(x,y) = q[-n(x,y) + p(x,y) + N_D^+(x,y) - N_A^-(x,y)] \tag{2}$$

$$-\frac{\hbar^2}{2}\nabla\cdot\left[\frac{1}{m^*}\nabla\Psi_n(x,y)\right] + V(x,y)\Psi_n(x,y) = E_n\Psi_n(x,y) \tag{3}$$

*Corresponding author. Tel.: +82-32-860-8686. Fax: +82-32-875-7436. Email: twon@hsel.inha.ac.kr

Molecular Simulation
ISSN 0892-7022 print/ISSN 1029-0435 online © 2005 Taylor & Francis
http://www.tandf.co.uk/journals
DOI: 10.1080/08927020500314076

where ε is the dielectric constant, Φ the electrostatic potential, ρ the total charge density, n and p the electron and hole concentrations, N_D^+ and N_A^- the ionized donor and acceptor concentrations, $\Psi_n(x,y)$ the wave function of nth eigenstates, $\hbar$ Planck's constant divided by 2π, $m^*(x,y)$ the effective mass, E_n the energy of nth eigenstates, and V the potential energy, which is given by $V(x,y) = \Delta E_c(x,y) - q\Phi(x,y)$. Here, $\Delta E_c(x,y)$ is the band offset in the conduction band. The densities of ionized donors and acceptors are expressed as

$$N_D^+(x,y) = \frac{N_D(x,y)}{1 + g_D\, e^{(E_{Fn}(x,y) - E_D)/k_B T}} \tag{4}$$

$$N_A^-(x,y) = \frac{N_A(x,y)}{1 + g_A e^{(E_A - E_{Fp}(x,y))/k_B T}} \tag{5}$$

where $N_D(x,y)$ and $N_A(x,y)$ are the donor and acceptor concentrations, g_D and g_A the degeneracy factors of the energy levels, $E_{Fn}(x,y)$ and $E_{Fp}(x,y)$ the quasi-Fermi levels, E_D and E_A the ionization energies of donor and acceptor, k_B the Boltzmann constant and T the temperature.

We used the mixed Dirichlet and von Neumann boundary conditions for the solution of Schrödinger equation which solve the Schrödinger equation with Dirichlet and Neumann boundary conditions respectively, and normalize the states to 1/2. The mixed Dirichlet and von Neumann boundary conditions are given by the following equation:

$$\int |\Psi(z)|^2 dz = 1/2 \tag{6}$$

This means that we obtain a constant function by summing cosine functions from Dirichlet boundary conditions and sine functions from von Neumann boundary conditions with normalization to 1/2.

By solving the Schrödinger equation, we obtain the quantized states which are occupied with the local quasi-Fermi levels. The 2D quantum electron density is found by using [5]

$$n(x,y) = \frac{1}{\pi\hbar}\sqrt{2m^* k_B T}\sum_j \left|\Psi_j(x,y)\right|^2 F_{-1/2}\left(\frac{E_F - E_j}{k_B T}\right) \tag{7}$$

where E_j and $\Psi_j(x,y)$ are the energy and the wave function of the jth eigenstate, $E_F(x,y)$ the Fermi level, and F_k the Fermi-Dirac integrals of order k. These integrals are defined as follows:

$$F_k(\eta) = \frac{1}{\Gamma(k+1)}\int_0^\infty \frac{u^k du}{1 + e^{u-\eta}}, \quad k \geq -1 \tag{8}$$

and also have the following property:

$$\frac{d}{d\eta}F_k(\eta) = F_{k-1}(\eta), \quad k \leq -1 \tag{9}$$

We obtain the semi-classical current solution from the 1st moment of the Boltzmann equation by adopting a simple drift-diffusion model for the electron current:

$$J_n(x,y) = \mu_n(x,y) n(x,y) \nabla E_{Fn}(x,y) \tag{10}$$

The continuity equation for current density is given by

$$\nabla \cdot J_n(x,y) = 0 \tag{11}$$

As per a model of carrier mobility, we employed physics-based and semi-empirical model which is taken various scattering mechanisms into account using Mathiessen rule [6].

$$\frac{1}{\mu} = \frac{1}{\mu_b} + \frac{1}{\mu_{ac}} + \frac{1}{\mu_{sr}} \tag{12}$$

where μ_b is the carrier mobility in bulk, μ_{ac} the carrier mobility from the surface acoustic phonon scattering, and μ_{sr} the carrier mobility from surface roughness.

The bulk mobility, μ_b, uses the empirical model expressed by Masetti *et al.* [7] which depends on the impurity concentration and temperature.

$$\mu_b(N_A, T) = \mu_0 + \frac{\mu_{max}(T) - \mu_0}{1 + (N_A/C_r)^\alpha} - \frac{\mu_1}{1 + (C_s/N_A)^\beta} \tag{13}$$

$$\mu_{max}(T) = \mu_{max}\left(\frac{T}{300}\right)^{-\gamma} \tag{14}$$

where N_A is the local acceptor concentration and $\gamma_{init} = 2.42$, the initial estimate for γ.

The electron mobility for the acoustic phonon scattering and nondegenerate surface, μ_{ac}, is expressed by [7]

$$\mu_{ac}(E_\perp, T) = \left(\frac{BT}{E_\perp} + \frac{C}{E_\perp^{1/3}}\right)\frac{1}{T} \tag{15}$$

where $E_\perp$ is the perpendicular electric field to the direction of current flow. Further, B and C are fitting parameters with initial values of $B_{init} = 3.1 \times 10^8$ cm/s and $C_{init} = 3.0 \times 10^7\,(\mathrm{V/cm})^{-2/3}\,\mathrm{K\,cm/s}$ based on physical quantities such as deformation potential, mass density of silicon, and effective thickness of inversion layer [8].

At very high perpendicular electric field, surface roughness scattering, μ_{sr} significantly affects the inversion layer mobility. It is described as follows [9]:

$$\mu_{sr}(E_\perp) = \frac{\delta}{E_\perp^2} \tag{16}$$

where δ is a constant depending on the oxide growth condition, and the initial value of δ is $\delta_{init} = 6 \times 10^{14}\,\mathrm{V/s}$. We consider the decrease of surface roughness scattering of CC-NMOS by specifying the μ_{sr} of equation 12 and include the velocity overshoot effect of strained-Si and dependence of Ge concentration [10].

For the above carrier mobility model, we have arranged the optimized results for the model fitting parameters in table I for electrons and holes.

Table 1. Mobility model parameters.

Parameter	*Electrons*	*Holes*	*Units*
μ_0	52.2	44.9	$cm^2/V\ s$
μ_{max}	1417	470.5	$cm^2/V\ s$
μ_1	43.4	29.0	$cm^2/V\ s$
C_r	9.68×10^{16}	2.23×10^{17}	cm^{-3}
C_s	3.43×10^{20}	6.10×10^{20}	cm^{-3}
α	0.680	0.719	–
β	2.00	2.00	–
γ	2.5	2.2	–
B	4.75×10^7	9.93×10^7	cm/s
C	$1.74 \times 10^5 \times N_A^{0.125}$	$8.84 \times 10^5 \times N_D^{0.125}$	N_A in cm^{-3}
δ	5.82×10^{14}	2.05×10^{14}	–

From Ref. [7].

In order to obtain self-consistent QM solutions, we have employed an iterative procedure [11]. We start out by calculating the electric potential. Next, the program calculates a charge distribution by using an iteration scheme. Thereafter, the program determines self-consistent solutions of Poisson–Schrödinger and current equations [11]. The Newton method has been employed called conjugate gradient method with a constraint that should satisfy error criteria as outlined in [12]. The discretization of main equations is performed through box-integration method to apply the finite difference method. The flow diagram of the quantum-mechanical simulation is demonstrated in figure 1.

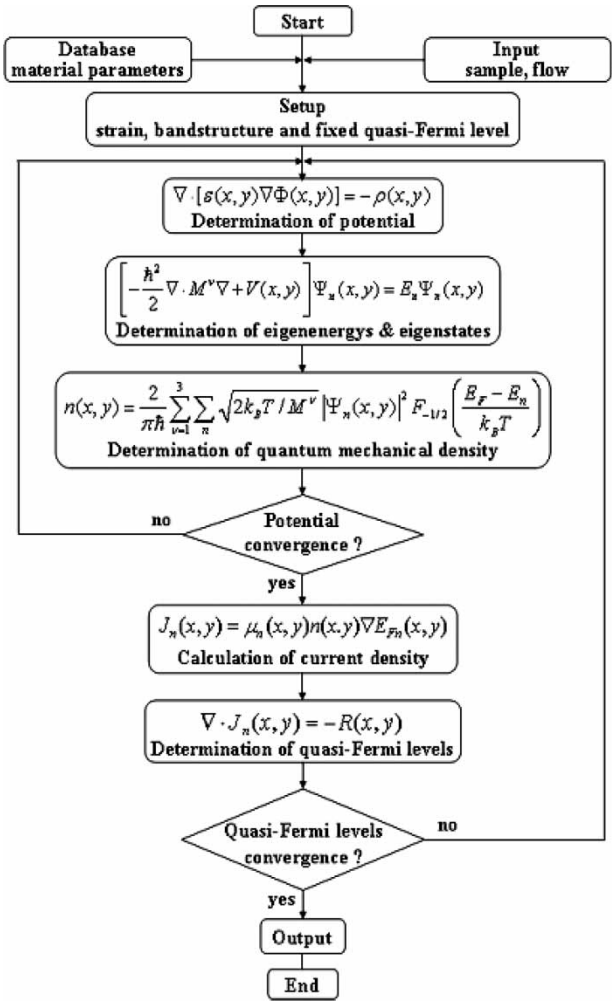

Figure 1. Flow diagram of the quantum-mechanical simulation.

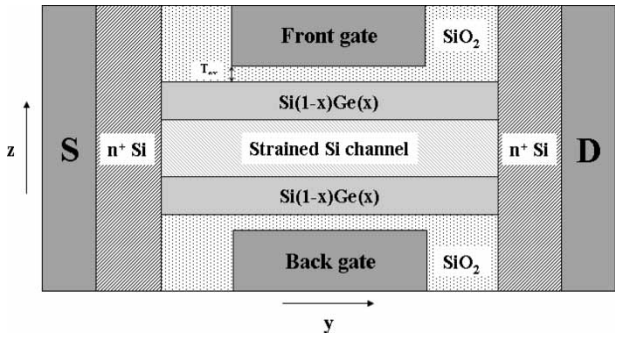

Figure 2. Schematic diagram of CC-NMOS considered in this work.

Figure 2 schematically shows the CC-NMOS considered in this work. Two metal gates with gate length L_g and work function $\Phi_M = 4.1$ eV are located symmetrically on both sides of $Si_{1-x}Ge_x/Si/Si_{1-x}Ge_x$ heterostructure. The source and drain regions are modeled as ohmic contacts with a doping of $2 \times 10^{20}/cm^3$, and the channel region under the gate is undoped. The oxide thickness (T_{ox}) is 2 nm, and L_g varies from 10 to 80 nm.

3. Simulation results

In this work, we confirmed the CC operation, the enhancement of drive current and G_m, and short-channel effects (SCE) of the proposed CC-NMOS structure.

First, we confirmed the CC operation of CC-NMOS through the band lineups, lowest energy wavefunction, and electron density. Figure 3 shows the comparison of conduction band lineups of CC and DG-NMOS with $L_g = 30$ nm, $V_d = 0.1$ V, and $V_g = 1.5$ V. From this result, we understand the difference of band offsets in CC and

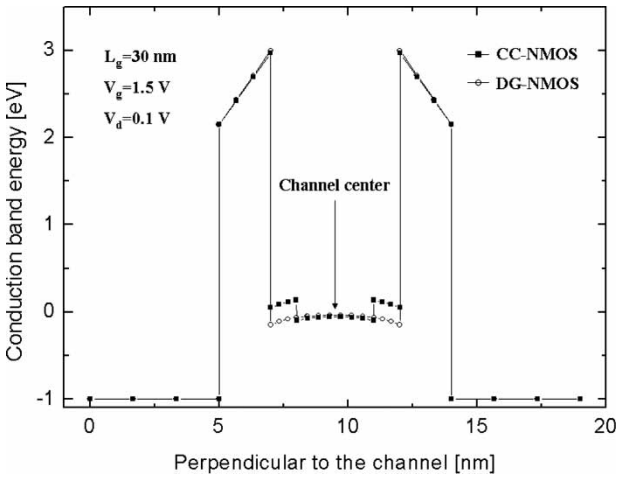

Figure 3. Comparison of band lineups of CC and DG-NMOS for $L_g = 30$ nm, $V_d = 0.1$ V, and $V_g = 1.5$ V.

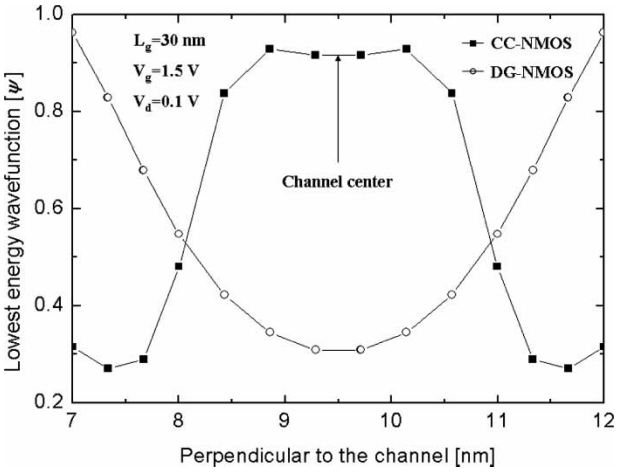

Figure 4. Comparison of lowest energy wavefunction of CC and DG-NMOS for $L_g = 30\,\text{nm}$, $V_d = 0.1\,\text{V}$.

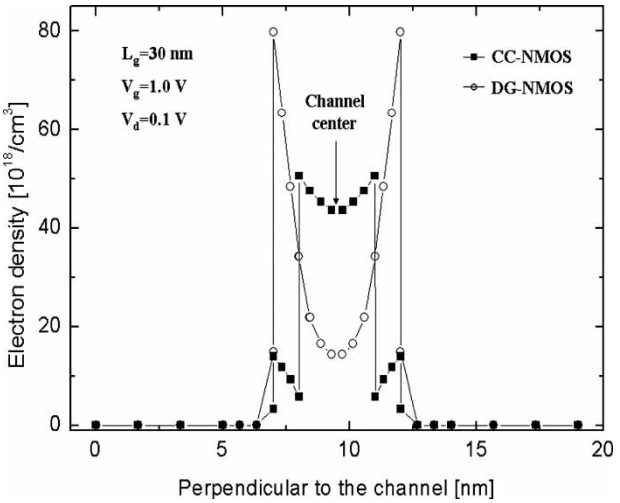

Figure 6. Comparison of electron density of CC and DG-NMOS for $L_g = 30\,\text{nm}$, $V_d = 0.1\,\text{V}$, and $V_g = 1.0\,\text{V}$.

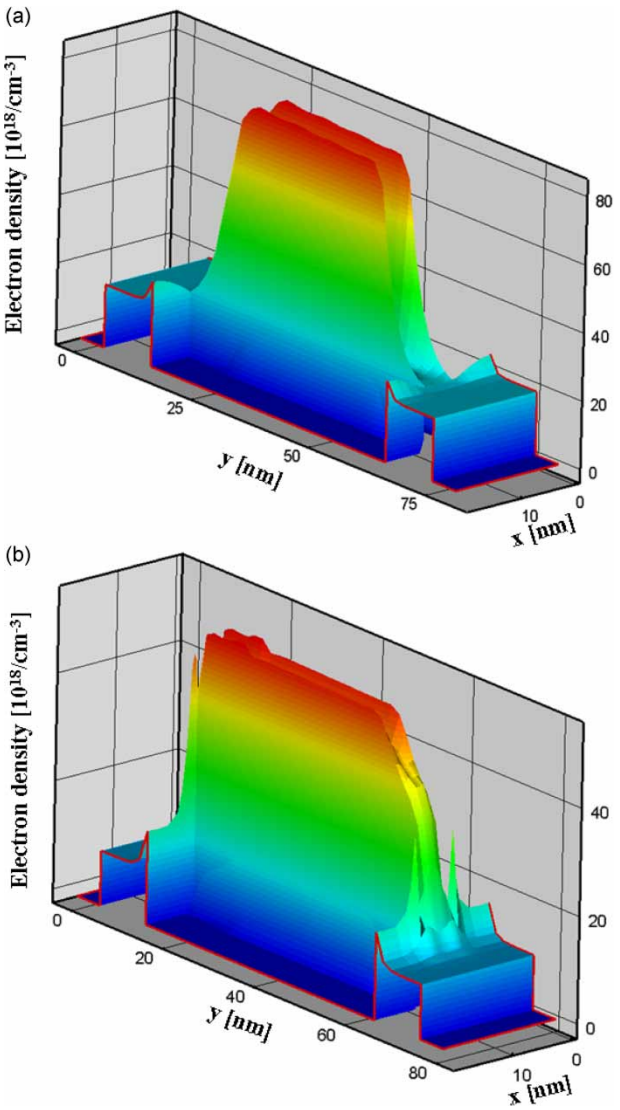

Figure 5. Quantum electron density for $L_g = 30\,\text{nm}$, $V_d = 0.1\,\text{V}$, and $V_g = 1.0\,\text{V}$. (a) DG-NMOS, (b) CC-NMOS.

DG-NMOS, the formation of quantum-well of CC-NMOS from $Si_{1-x}Ge_x/Si/Si_{1-x}Ge_x$ heterostructure, and corresponding CC operation. The lowest energy wavefunction of CC-NMOS is compared with that of DG-NMOS in figure 4 at the condition of $L_g = 30\,\text{nm}$, $V_d = 0.1\,\text{V}$, and $V_g = 1.5\,\text{V}$. Contrary to DG-NMOS, the wavefunction of CC-NMOS is confined to the center of channel meaning the CC operation.

Figure 5 shows quantum electron density for $L_g = 30\,\text{nm}$, $V_d = 0.1\,\text{V}$, and $V_g = 1.0\,\text{V}$: (a) DG-NMOS, (b) CC-NMOS. The electron density of DG-NMOS shows the peak value at the both side of channel. On the other hand, the electrons of CC-NMOS are confined at the center of $Si_{1-x}Ge_x/Si/Si_{1-x}Ge_x$ heterostructure which are definitely shown the CC operation. And the cross sections as seen for a cut through the Si channel of CC and DG-NMOS quantum electron densities are compared in figure 6. These results visibly show the different shape of channels in CC and DG-NMOS.

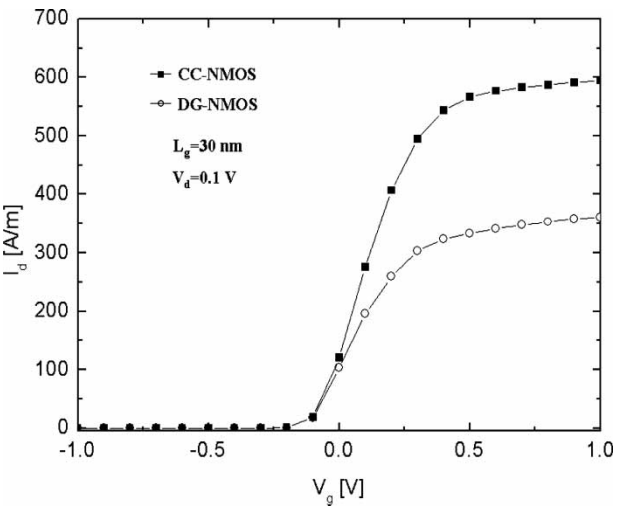

Figure 7. I_d–V_g characteristics of CC and DG-NMOS for $L_g = 30\,\text{nm}$, $V_d = 0.1\,\text{V}$.

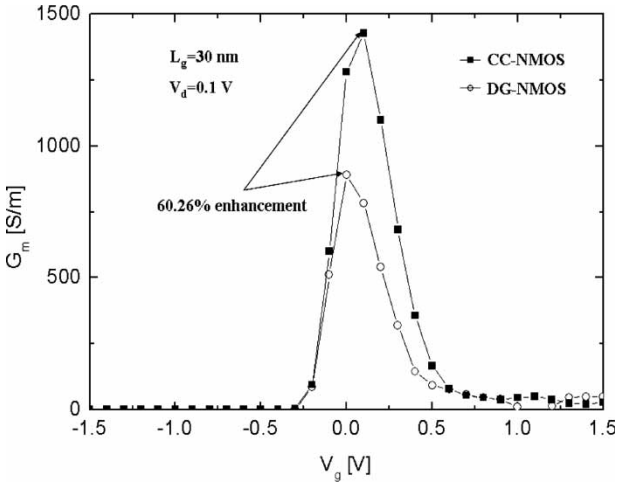

Figure 8. G_m characteristics of CC and DG-NMOS for $L_g = 30$ nm, $V_d = 0.1$ V

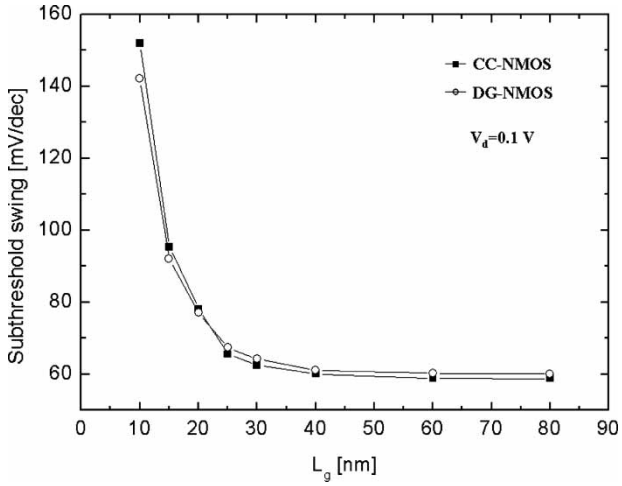

Figure 10. Subthreshold swing of CC and DG-NMOS in terms of L_g at $V_d = 0.1$ V.

Figure 7 demonstrates the comparison of current–voltage (I_d–V_g) characteristics of CC and DG-NMOS at the condition of $L_g = 30$ nm and $V_d = 0.1$ V. This simulation result shows the enhancement about $\sim 1.6\times$ current drive. And the transconductances (G_m) of CC and DG-NMOS are compared in figure 8. The G_m of CC-NMOS increases about 60% comparing with that of DG-NMOS which shows $G_m = 1428.3$ S/m at CC-NMOS, $G_m = 891.3$ S/m at DG-NMOS. It is due to the enhancement of carrier mobility caused by the strained-Si and the decrease of surface roughness scattering.

Finally, we estimated the SCE of CC and DG-NMOS by performing the simulation with respect to L_g. Figure 9 show the I_d–V_g curves for CC-NMOS performed under the condition of L_g varying from 10 nm to 80 nm at $V_d = 0.1$ V. As the L_g decreases, the short channel behavior is visibly come in sight. Therefore, we analyze the SCE in terms of subthreshold swing, threshold voltage (V_t) roll-off, drain-induced barrier lowering (DIBL). Figure 10 shows the subthreshold swing of CC and DG-NMOS in terms of L_g at $V_d = 0.1$ V. And, V_t roll-off and DIBL characteristics are demonstrated in figure 11. From these results, we confirmed that both CC and DG-NMOS show excellent subthreshold behaviors and successfully suppress the SCE.

4. Conclusion

In this paper, we discussed our two-dimensional numerical modeling and simulation results for center-channel (CC) double-gate (DG) MOSFET with comparison to those of conventional DG structure. CC operation of CC-NMOS is confirmed by band lineups, lowest energy wavefunction, and electron density. The simulation results also reveal that current drive and transconductance are remarkably enhanced and the short-channel effects are appreciably

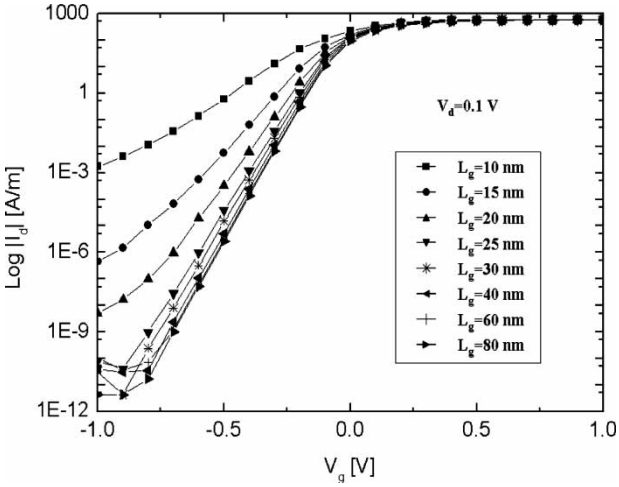

Figure 9. I_d–V_g characteristics for CC-NMOS with L_g of 10–80 nm, $V_d = 0.1$ V.

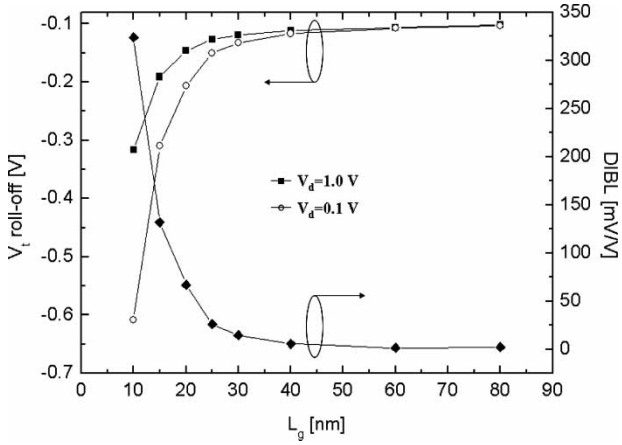

Figure 11. I_d–V_g V_t roll-off and DIBL of CC-NMOS in terms of L_g.

suppressed. Our simulation results imply that CC-NMOS structure is a promising candidate for implementing the sub-20 nm MOSFETs.

Acknowledgements

This work was supported partly by the Korean Ministry of Information & Communication (MIC) through the Information Technology Research Center (ITRC) Program supervised by IITA, and partly by the Korean Ministry of Science and Technology (MOST) through the Tera-Nano Development (TND) Program and the Nano Core Basic Research Program (M1-0213-04-0002) by KISTEP.

References

[1] T. Krishnamohan, C. Jungemann, K.C. Saraswat. Very high performance, Sub-20 nm, strained Si and Si_xGe_{1-x}, Hetero-Structure, Center Channel (CC) NMOS and PMOS DGFETs. *SISPAD Tech. Dig.*, 191 (2004).

[2] A. Svizhenko, M.P. Anantram, T.R. Govindan, B. Biegel. Two-dimensional quantum mechanical modelling of nanotransistors. *J. Appl. Phys.*, **91**(4), 2343 (2002).

[3] S.H. Jin, Y.J. Park, H.S. Min. Simulation of quantum effects and nonlocal transport by using the hydrodynamic density-gradient model. *J. Korean Phys. Soc.*, **44**, 87 (2004).

[4] K. Kim, O. Kwon, J. Seo, T. Won. Two-dimensional quantum effects and structural optimization of FinFETs with two-dimensional Poisson–Schrődinger solver. *J. Korean Phys. Soc.*, **45**, 1384 (2004).

[5] A. Trellakis, A.T. Galick. Iteration Scheme for the solution of the two-dimensional Schrődinger–Poisson equations in quantum structures. *J. Appl. Phys.*, **81**(15), 7880 (1997).

[6] I.H. Cho, B.G. Park, J.D. Lee, J.H. Lee. Nano-Scale SONOS memory with a double-gate MOSFET structure. *J. Korean Phys. Soc.*, **42**, 233 (2003).

[7] G. Masetti, M. Severi, S. Solmi. Modeling of carrier mobility against carrier concentration in arsenic-, phosphorus- and boron-doped silicon. *IEEE Trans. Electron Devices*, **30**(7), 764 (1983).

[8] C.T. Sah, T.H. Ning, L.L. Tschopp. The scattering of electrons by surface oxide charges and by lattice vibrations at the silicon-silicon dioxide interface. *Surf. Sci.*, **32**, 561 (1972).

[9] C. Lombardi, S. Manzini, A. Saporito, M. Vanzi. A physically based mobility model for numerical simulation of nonplanar devices. *IEEE Trans. Comput.-Aided Desi.*, **7**(11), 1164 (1988).

[10] F.M. Bufler, W. Fichtner. Scaling of strained-Si n-MOSFETs into the ballistic regime and associated anisotropic effects. *IEEE Trans. Electron Devices*, **50**(2), 278 (2003).

[11] M. Sabathil, S. Hackenbuchner, J.A. Majewski, G. Zandler, P. Vogl. Towards fully quantum mechanical 3D device simulation. *Comput. Electron*, **1**, 81 (2002).

[12] S.E. Laux, A. Kumar, M.V. Fischetti. Ballistic FET modeling using QDAME: quantum device analysis by modal evaluation. *IEDM Tech. Dig.*, 715 (2002).